Aging blood factors promote CD8$^+$ T cell infiltration in the adult mouse brain

Lynn van Olst (l.vanolst@amsterdamumc.nl)
Amsterdam UMC https://orcid.org/0000-0001-7569-0470
Alwin Kamermans
Amsterdam UMC location VUmc https://orcid.org/0000-0002-3601-395X
Susanne van der Pol
Amsterdam UMC
Lianne Hulshof
University Medical Centre Utrecht
Roland van Dijk
University Medical Centre Utrecht
Danielle Vonk
University Medical Centre Utrecht
Marijn Schouten
Amsterdam UMC
Maarten Witte
Amsterdam UMC https://orcid.org/0000-0002-1407-6220
Helga de Vries
Amsterdam UMC
Jinte Middeldorp
Biomedical Primate Research Centre

Article

Keywords:

Posted Date: January 25th, 2022

DOI: https://doi.org/10.21203/rs.3.rs-1266205/v1

Abstract

Aging coincides with major changes in brain immunity that aid in a decline in neuronal function. Here, we postulate that systemic, pro-aging factors contribute to immunological changes that occur within the brain during aging. To investigate this hypothesis, we first characterized the immune landscape upon aging in 20-month-old mice using cytometry by time-of-flight (CyTOF) and observed that memory T cells expanded in the circulation and that specifically effector $CD8^+$ T cells expressing programmed cell death protein 1 (PD-1) and tissue-resident memory $CD8^+$ T cells accumulated in the aged brain. Injections of plasma derived from 20-month-old mice into 5-month-old receiving mice decreased the frequency of splenic and circulating naïve T cells, increased memory $CD8^+$ T cells and non-classical, patrolling monocytes in the spleen, and elevated levels of regulatory T cells and non-classical monocytes in the blood. Finally, we found an accumulation of $CD8^+$ T cells within the brain parenchyma of plasma-treated mice, which coincided with expression of vascular cell adhesion molecule 1 (VCAM-1), a mediator of immune cell trafficking, on the brain vasculature and increased numbers of proliferating microglia. Taken together, our data highlight a role for $CD8^+$ T cells in the aged brain and suggests involvement of age-associated systemic factors that mediate $CD8^+$ T cell migration and expansion in the brain parenchyma.

Introduction

During aging, the immune system becomes less efficient in mounting an effective response against pathogens and harmful processes such as the accumulation of senescent cells, misfolded proteins and cellular degeneration. This decline in immune function, called immunosenescence, has also been associated with age-related neurodegenerative diseases like Alzheimer's disease (AD) and AD-related dementias[1] and goes hand-in-hand with an increase in basal levels of inflammatory factors, a phenomenon known as inflammaging[2].

The brain its immune system mainly consists out of its own unique immune cells, microglia, and harbors relatively low numbers of peripheral immune cells as T, B and natural killer (NK) cells, neutrophils, macrophages, dendritic cells (DCs) and other myeloid-derived cells (MdCs)[3,4]. During aging however, peripheral immune cells increasingly infiltrate and expand in the brain[4]. Memory T cells[5] and specifically $CD8^+$ T cells[6,7,8] accumulate in the brain during aging where they modify microglia homeostasis and can potentiate inflammation and leukocyte recruitment. Interestingly, $CD3^+$ T cells found in the aged brain are clonally expanded and exhibited higher interferon-γ signaling than their peripheral counterparts, indicating antigen experience[9]. In AD patients, $CD8^+$ T cells have been increasingly found in the cerebral spinal fluid and brain parenchyma[10,11] which coincided with higher numbers of circulating effector memory $CD8^+$ T cells that negatively associated with cognition[11]. Next to memory T cells, a subset of circulating B cells, termed age-associated B cells, accumulates in the elderly as well[12] and B cell depletion strategies ameliorated disease progression in an AD model[13]. Together, these studies provide strong

evidence that aging and age-related diseases as AD are associated with changes in adaptive immune cells in both the circulation and the brain.

Local and distant immune communication is tightly controlled through cell-cell contacts and via numerous soluble systemic factors like cytokines, hormones and growth factors, among others. During the human lifespan, the plasma proteome shows three waves of changes, reflecting aspects of aging of different cell types and tissues[14]. In aged mice, blood plasma contained higher levels of pro-inflammatory cytokines and chemokines which affect brain function[15]. Parabiosis experiments have shown that an aged systemic environment negatively impacts neurogenesis, cognitive function and activates microglia of young mice[15,16]. Contrariwise, plasma derived from young and physical active mice is able to rejuvenate multiple tissues including the brain[17–19] and rescue neuroinflammation and neurodegeneration in a mouse model for AD and acute brain inflammation[17,20].

Still, despite efforts made to dissect underlying age-related immune changes that contribute to neurodegeneration, parts of the puzzle remain incomplete. Here, we profiled immune cells using cytometry by time-of-flight (CyTOF) of the blood and brain of old and young-adult mice and investigated if exposure to plasma derived from old mice induces age-related immunological changes in younger adult mice. Altogether, our data show that normal aging changes both the immune landscape of the brain and the periphery and these changes can be (partly) mimicked by exposing younger mice to plasma of aged mice.

Results

Aging changes the peripheral immune landscape

We first determined the impact of aging on circulating immune cell populations within the blood of old mice (20 months) by comparing it to younger adult mice (6 months) (Fig. 1a). Immune cells isolated from the blood were stained with a 37-heavy metal isotope-tagged antibody panel for mass cytometry containing surface and nuclear markers to define immune cell populations (Table 1). Data were visualized in a UMAP (Fig. 1b) and cells were appointed to clusters by Phenotyping by Accelerated Refined Community[21] (PARC). Finally, PARC-derived clusters were manually merged into biologically relevant immune cell subsets (Fig. S1a).

B cells increased in frequency at the expense of all myeloid cell populations (e.g. monocytes, neutrophils, eosinophils and myeloid-derived cells (MdCs)) in the circulation of old mice (Fig. 1c) and expressed higher levels of CX3CR1 (Fig. S1b). $CD8^+$ T cells as a percentage of $CD45^+$ immune cells did not change, while the proportion of $CD4^+$ T cells decreased (Fig. 1c). Within myeloid cells we detected a lower frequency of classical, inflammatory $Ly6C^{high}$ monocytes while eosinophils took up a larger proportion (Fig. 1d). Among T cells, $CD8^+$ T cells increased in percentage whereas $CD4^+$ T cells decreased in old mice (Fig. 1e). More in depth phenotyping of T cells (Fig. 1f-g) showed an increase in $CD4^+$ and $CD8^+$ memory T cells expressing $CD44^+$ $CD127^+$ at the expense of $CD44^-$ $CD127^+$ naïve populations and an

increase in $CD8^+$ effector T cells defined as $CD44^+$ $CD127^-$ (Fig. 1h). Memory $CD8^+$ T cells ($CD8^+$ mem), the most abundant circulating T cell population in old mice, $PD1^+$ $KLRG1^-$ effector $CD8^+$ T cells ($CD8^+$ eff1), $Ly6C^-$ memory $CD4^+$ T cells ($CD4^+$ mem1) and NKT cells were increased old mice, while the proportion of $CD44^{low}$ $KLRG1^-$ $CD103^-$ quiescent regulatory T cells (Tregs; $CD4^+$ treg1) and of all gamma delta T cells (γδ T cells) decreased (Fig. 1i). Altogether, the aged peripheral landscape is marked by a high proportion of B cells and a decline in myeloid subsets. Within the T cells, effector and especially memory populations were increased at the expense of naïve, regulatory and γδ T-cell subsets.

Aging changes the brain immune landscape

Next, we investigated how the brain immune landscape changed with aging. For this purpose, immune cells were isolated from the brain of old (20 months) and younger adult (6 months) mice, stained with our CyTOF antibody panel and subsets were characterized (Fig. 2a-b; Fig. S1c). Upon aging, the absolute number of non-microglial immune cells quadrupled, while numbers of microglia remained the same (Fig. 2c). Consequently, every non-microglial immune cell type we were able to detect was enriched in the total pool of immune cells (Fig. S1d). Among the non-microglial immune cells in the aged brain, specifically B cells, plasma cells and neutrophils accumulated (Fig. 2d). In addition, B cells derived from the brain of old mice expressed higher levels of LFA1, CD5 and CD38 (Fig. S1e). Concomitantly, a subset of border-associated macrophages (BAMs), which include macrophages resident in the perivascular spaces of brain vessels, lining the meninges, and the choroid plexus[4] and DCs decreased in old mice together with NK cells (Fig. 2d). BAMs can be further subdivided based on CD38 and MHC class II (MHCII) expression[4]. Imputing the subset of BAMs and DCs for further sub-clustering revealed different subsets of BAMs within the brain (Fig. 2e-f) and a shift towards more $CD38^+$ $MHCII^+$ BAMs in the aged brain at the expense of $CD38^-$ $MHCII^+$ BAMs (Fig. 2g). Conventional DCs (cDCs) can be divided into two major subsets called cDC1s and cDC2s. cDC1s engage in cross-presentation or the priming of naive $CD8^+$ T cells through MHCI, while cDC2s are specialized in co-stimulation and induce naïve $CD4^+$ T cells through presentation on MHCII. Within the pool of DCs, cDC1s were increased in the aged brain, while cDC2s decreased and the percentage of monocyte-derived DCs (moDCs) remained unchanged (Fig. 2h). Together, these data show that non-microglial immune cells accumulate in the brain during aging, and that the frequency of B cells, plasma cells, neutrophils, BAMs, DCs and NK cells changes among the brain-immune infiltrates.

Subsets of $PD1^+$ effector and memory T cells accumulate in the aged brain

Next, we investigated if aging changed dominancy of certain $CD8^+$ and $CD4^+$ subsets in the brain. Briefly, T cells were re-clustered, and naïve, effector and memory phenotypes were assigned when possible (Fig. 2i-j). With aging, the proportion of $CD8^+$ T cells increased in the brain as a percentage of all T cells (Fig. 2k). Among $CD4^+$ T cells, naïve cells decreased while the fraction of memory $CD4^+$ T cells expanded (Fig. 2k). A closer look into T-cell subsets within $CD8^+$, $CD4^+$ and double-negative (DN) T cells showed a striking expansion of $CD8^+$ $PD1^+$ effector T cells ($CD8^+$ eff3) in the brain from 2.2% ± 1.5% in adult mice to 18.6% ± 3.6% in old mice (Fig. 2l). This '$CD8^+$ eff3' effector population was very similar to the $PD1^+$

effector $CD8^+$ T cells found increased in the blood of old mice before ($CD8^+$ eff1; Fig. 1i). The aged brain harbored higher levels of $CD103^+$ tissue-resident memory $CD8^+$ T cells ($CD8^+$ trm), $Ly6C^-$ $CX3CR1^-$ memory $CD4^+$ T cells ($CD4^+$ mem3) and $ICOS^+$ $PD1^+$ Tregs ($CD4^+$ treg1; Fig. 2l). In addition, the frequency of $Ly6C^-$ $KLRG1^-$ $PD1^-$ effector $CD8^+$ T cells ($CD8^+$ eff4), $Tbet^-$ $PD1^-$ effector $CD4^+$ T cells ($CD4^+$ eff2), $CX3CR1^{high}$ $Ly6C^-$ highly polarized cytotoxic effector memory $CD4^+$ T cells ($CD4^+$ mem1) and $Ly6C^+$ DN T cells (DN2) was decreased in the aged brain (Fig. 2l). In sum, the aged brain reflects partly age-associated changes in circulating immune subsets, including the expansion of $PD1^+$ effector $CD8^+$ T cells, memory T cells and the decline in naïve T-cell subsets, but in contrast to the blood, also harbors an increased frequency of $ICOS^+$ $PD1^+$ regulatory T cells.

Aged plasma increases $Ly6C^{low}$ $PDL1^+$ non-classical monocytes and memory $CD8^+$ T cells in the periphery

We show that aging rearranges the composition of immune cells in the circulation and that the brain reflects parts of these changes. Next, we hypothesized that exposure to age-associated systemic factors might drive these shifts in peripheral and central immunity. To investigate this, 5-month-old mice were exposed to blood plasma derived from 20-month-old mice (termed: ‘aged plasma’) biweekly for 4 weeks (Fig. 3a). Then, immune cells were isolated from the spleen, the largest blood filtrating secondary lymphoid organ, and from the blood, where after immune cell populations were defined using our CyTOF panel (Fig. 3b-c; Fig. S2a-c). Treatment with aged plasma increased the frequency of splenic and circulating $Ly6C^{low}$ $PDL1^+$ non-classical monocytes (Fig. 3d), also known as non-classical patrolling monocytes, but not that of other immune populations (Fig. S2d-f). Among peripheral T cells (Fig. 1e-f; Fig. S3a-d), exposure to aged plasma decreased the frequency of naïve $CD8^+$ T cells in both spleen and blood, and of naïve $CD4^+$ T cells in blood only (Fig. 3g-h), mimicking our earlier findings in old mice (Fig. 1h). In the spleen, the decrease in naïve $CD8^+$ T cells was concomitant with an increase in memory $CD8^+$ T cells (Fig. 3g). Specifically, aged plasma increased a population of splenic $Ly6C^+$ $Tbet^{dim}$ memory $CD8^+$ T cells that expressed co-inhibitory molecule TIGIT ($CD8^+$ mem2; Fig. 3i), while $CD44^{low}$ $KLRG1^-$ $CD103^-$ quiescent Tregs increased in the circulation ($CD4^+$ treg2; Fig. 3j). The latter finding in contrast to the circulation of aged animals, where this regulatory T cell population was decreased ($CD4^+$ treg1; Fig. 1i). Together, these findings show that aged systemic factors increase levels of non-classical monocytes in the spleen and circulation, and raise levels of splenic memory $CD8^+$ $TIGIT^+$ T cells and of circulating quiescent Tregs.

Aged plasma induces $CD8^+$ T cell and plasmacytoid DC accumulation in the brain

Next, we set out to find if aged plasma also induced, either directly or indirectly, immune changes within the brain parenchyma. First, immune cells were isolated from the brains of aged plasma-treated mice and phenotyped using CyTOF (Fig. 4a-b; Fig. S4a). While the ratio between microglia and non-microglial immune cells was not affected (Fig. 4c), we found that the frequency of $CD3^+$ $CD4^-$ T cells, presumably $CD8^+$ T cells, doubled in the brain of aged plasma-treated mice (Fig. 4d). $CD3^+$ $CD4^+$ T cells and other

subsets of non-microglial immune cells derived from the initial clustering did not change (Fig. 4d; Fig. S4b). Deeper phenotyping of BAMs, DCs and T cells revealed however an increase in plasmacytoid DCs (pDCs; Fig. 4e-g), which are prominent secretors of type 1 interferons (IFNs). Among $CD3^+$ T cells, further subsetting revealed an increase $Ly6C^+$ $CD4^-$ T cells that expressed LFA1 (Fig. 4h-i), a common marker of effector/memory T cells. Immunohistochemical analysis confirmed the infiltration of $CD45^+$ immune cells and $CD45^+$ $CD8^+$ T cells in the brain parenchyma after aged plasma exposure, while numbers of $CD45^+$ $CD4^+$ T cells were less affected (Fig. 4j-k). Trafficking of immune cells into the brain is regulated by cell adhesion molecules on the brain vasculature such as VCAM-1. In line with previous findings[16], we found that aged plasma increased the number of $VCAM\text{-}1^+$ vessels in young-adult animals (Fig. 4l-m), whereas levels of ICAM-1 and PECAM-1 were not changed (Fig. S4c-h). Higher levels of $CD45^+$ immune cell infiltrates in the brain parenchyma correlated modestly ($r = 0.65$), but on a trend level ($P = 0.08$), to the increase in $VCAM\text{-}1^+$ vessels in the plasma-treated animals (Fig. 4n) and moderate or not to levels of PECAM-1 and ICAM-1, respectively (Fig. S4e, h). Aged plasma did not affect vascular permeability, as assessed by fibrinogen, a blood coagulation protein deposited in the brain upon vascular dysfunction (Fig. S4i-j), nor vessel density (Fig. S4l). In addition, vascular permeability was not related to increased numbers of $CD45^+$ immune cell infiltrates (Fig. S4k). Altogether, these findings indicate that pro-aging factors in plasma increase specifically pDCs and $CD8^+$ T cells in the brain and might facilitate immune cell trafficking of T cells into the brain via VCAM-1 expression on the brain vasculature.

Aged plasma increases the number of proliferating microglia but does not cause synaptic loss

To investigate if aged plasma would also affect the number and phenotype of microglial and neuronal cells, animals were injected for 3 consecutive days with 5'-bromo-2'-deoxyuridine (BrdU), which is incorporated into DNA during S-phase, starting the day after the last aged plasma injection. Interestingly, we found that aged plasma increased absolute numbers of cortical $BrdU^+$ $IBA1^+$ proliferating microglia cells (Fig. 5a-b) but did not raise levels of $BrdU^+$ $IBA1^+$ microglia in the hippocampus (Fig. 5c). Neither did aged plasma affect the proliferation of $IBA1^-$ cortical or hippocampal cells (as astrocytes, neurons, oligodendrocytes, endothelial cells, etc.; Fig. 5b-c), change numbers of $BrdU^+$ cells in the meninges (Fig. 5d) or affected the overall microglial density (Fig. 5e-g). Aged plasma exposure did however decrease microglial expression of homeostatic marker P2Y12 in the hippocampus (Fig. 5h-i), while microglial morphological features were unaffected (Fig. 5j-l). Aged plasma has shown to induce memory deficits in adult mice before[15], however, we did not find a loss of $Homer1^+$ post-synapses in the stratum radiatum of the hippocampus (Fig. 5m-n), nor a change in synaptic pruning by microglia (Fig. 5o) or in microglial lysosomal size (Fig. 5p. In addition, we did not observe cortical neuronal loss (Fig. 5q-r). Altogether, these data show that aged plasma increases the number of proliferating cortical microglia and reduced hippocampal microglial P2Y12 expression, but does not impact the loss of cortical neurons nor changed the amount of hippocampal post-synapses, or their pruning by microglia.

Discussion

We here systematically assessed age-associated changes in the immune landscape of the mouse circulation and brain and investigated whether exposure to aged plasma could induce similar changes in younger adult mice. We observed that the immune profile of aged mice is dominated by B cells and memory T cells and that circulating and brain-resident T cells of old animals show an exhausted phenotype, indicated by increased expression of PD1. Exposure of young-adult mice to plasma from aged animals mimicked the decrease in naïve T cells and increase in memory T cells in the periphery, and raised numbers of $CD8^+$ T cells within the brain parenchyma. The latter coinciding with increased VCAM-1 on the brain vasculature. In addition, exposure to aged plasma increased the fraction of splenic and circulating non-classical monocytes, of pDCs amongst brain-derived immune cells and augmented numbers of proliferating cortical microglia. Altogether, our data provides an in-depth characterization of immune cells, particularly T-cell subsets, present in the circulation and brain of old mice and indicates that systemic, pro-aging factors drive, at least partly, $CD8^+$ T cell infiltration in the aged brain. In addition, we establish new and validate previously found changes associated with aging in other immune subsets (e.g. B, NK, DC and myeloid cells).

Immune cells from the circulation and brain of aged animals showed a decline in the $CD4^+$:$CD8^+$ ratio, particularly due to increased numbers of memory $CD8^+$ T cells. Recent studies show that $CD8^+$ T cells are also elevated in the aged human brain[7,8] and even more in the circulation and brain of AD patients[10,11]. Specifically, tissue-resident memory T cells, which have been found in the elderly human brain before[5], accumulated in the aged mouse brain. We also found $PD1^+$ effector $CD8^+$ T cells that highly expressed CD38 to be increased in the circulation and brains of old mice. $CD38^+$ T cells are associated with recent activation[22] and lower cytotoxic capacity[23], while the $PD1^{high}$ subset is associated with $CD8^+$ T cell dysfunction and exhaustion[24]. In addition, a population of $ICOS^+$ $PD1^+$ Tregs expanded in the aged mouse brain. ICOS expression marks an activated regulatory subset with strong inhibitory capacity[25], but in combination with PD1 expression also associates with Treg exhaustion and increased IFN-γ secretion[26]. Future research should reveal whether high levels of $PD1^+$ effector $CD8^+$ T cells and exhausted Tregs in the aged brain present dysfunctional T cells that are unable to yield effective T cell responses and leave the brain vulnerable to external stressors. In addition, we found that the frequency of B cells and plasma cells highly increased with age in both the circulation and brain. Circulating B cells of aged mice showed increased expression of CX3CR1, which has been previously linked to B-cell mediated immunosuppression[27], while B cells in the aged brain expressed higher levels of LFA1, CD5 and CD38, which associate with B cell receptor (BCR) signaling and B cell activation[28–30]. Taken together, our data shows that B cells and memory T cells are increasingly present in the aged mouse blood and brain, and that different T-cell subsets show signs of exhaustion with high expression of inhibitory PD1.

Aged blood harbors increased levels of immune-derived cytokines and chemokines that have detrimental effects on the brain[15]. In an attempt to uncover if blood-borne factors present in the systemic milieu can induce the age-dependent immune changes found before, we repeatedly exposed young-adult mice to aged plasma for a duration of 4 weeks. These repeated injections led to an overall decline in circulating

$CD4^+$ and $CD8^+$ naïve T cells and of naïve splenic $CD8^+$ T cells while splenic $CD4^+$ T cell populations did not change. Exposure to aged plasma also increased memory $CD8^+$ T cells in the spleen, of which specifically $Tbet^{dim}$ memory T cells that also expressed Ly6C and TIGIT. Ly6C is expressed by most central memory $CD8^+$ T cells[31] which provide central immune immunosurveillance, sustain immune responses by proliferation in secondary lymphoid organs like the spleen, have a long-term survival and are suppliers of new effector memory cells[32]. TIGIT is a co-inhibitory molecule that can protect T cell recall responses by restricting terminal differentiation[33] and was upregulated on T cells from aged mice who exhibited features of exhaustion[34]. In contrast to our old mice however, aged plasma increased levels of circulating naïve $CD103^-$ $KLRG1^-$ Tregs as well. Finally, aged plasma exposure corroborated the age-associated reduction in $Ly6C^{high}/Ly6C^{low}$ monocyte ratio by elevating levels of circulating and splenic $Ly6C^{low}$ $PDL1^+$ non-classical monocytes. Non-classical monocytes engage in long-term migration, also called patrolling, along the endothelium and often exert anti-inflammatory and homeostatic effects[35–37]. Together, our data shows that exposure to aged plasma mirrors some age-associated peripheral immune changes, including an overall decline in naïve T cells, an increase in memory $CD8^+$ T cells that upregulated expression of co-inhibitory molecules and a reduced $Ly6C^{high}$ inflammatory to $Ly6C^{low}$ patrolling monocyte ratio.

Interestingly, exposure to aged plasma also elevated numbers of $LFA1^+$ $Ly6C^+$ effector/memory $CD8^+$ T cells in the brains of plasma-treated mice. Due to the low number of cells in this cluster analysis, we were not able to make a distinction between effector or memory phenotypes. Interestingly, the increase of $CD8^+$ T cells in the brain parenchyma associated with increased VCAM-1 levels on the brain vasculature. The latter finding confirming earlier data in which plasma from both old mice and humans increased VCAM-1 expression on brain endothelial cells[16]. VCAM-1 binds to VLA-4, which is expressed by leukocytes and is used for tethering, firm adhesion and transmigration of leukocytes into the brain. We did not find upregulation of other adhesion molecules such as ICAM-1 or PECAM-1. Equivalent, others also did not detect increased levels of ICAM-1, E-selection and P-selectin on the brain vasculature after exposure to aged plasma nor during normal aging[16]. Fibrinogen leakage into the brain, which is indicative of brain vasculature leakage, was also not increased after aged plasma exposure. As such, aged plasma either directly or indirectly via ongoing inflammatory responses, induces VCAM-1 expression on the brain vasculature which associates with more effector/memory T cells in the brain parenchyma. In addition, we found that pDCs were increased in the brains of plasma-treated mice. pDCs are the main source of type I IFNs and directly impact T cell responses through antigen presentation. Interestingly, a type 1 IFN signature in the brain was associated with aging before and negatively affected brain function[38,39].

Recent research shows that $CD8^+$ T cells induce phenotypic changes in microglia and neurons[40] and are involved in the killing of neurons[41–43], inhibition of neural stem cell proliferation[9], synaptic elimination[44,45] and associate with a decline in synaptic plasticity and cognition in AD pathology[10,11]. Indeed, we found that aged plasma increased the number of proliferating microglia in the cortex, and decreased expression of the purinoceptor P2Y12 in hippocampal microglia, a homeostatic microglial

marker[46] that is involved in microglia-mediated neuronal regulation[47]. However, we did not observe synaptic or neuronal loss, nor altered synaptic pruning by microglia. Others have reported that aged plasma decreased hippocampal long-term potentiation, neurogenesis and performance on learning and memory tasks in younger mice of 2-3 months approximately[15,16,48]. Possibly, effects of aged plasma on neuronal and synaptic processes are more profound at earlier ages.

Future studies can now focus on identifying the factors in aged plasma that are responsible for the observed immunological changes. Since plasma was dialyzed prior to injection, most growth factors, lipids, metabolites and other small molecules were removed, leaving the main candidates responsible for the immunologic effects plasma-derived proteins such as cytokines, chemokines and hormones. We found that age-associated systemic factors in plasma mimicked the loss of naïve T cells and the expansion of memory T cells in the periphery, and reflected $CD8^+$ T cell accumulation in the brain. However, we did not find age-associated changes in B cells, NK cells or neutrophils after exposure to aged plasma. Maybe, these age-associated changes occur after prolonged plasma exposure or are induced by other aging factors that are not present in our aged plasma.

Earlier reports have characterized immune cells in the steady-state brain[3] and during aging and neurodegeneration[4]. These well performed studies changed our view of the brain as an immune privileged organ but focused mostly on defining different myeloid immune cell subsets, while T cells were not investigated in depth. Recent studies found that T cells play an important role in neurodegenerative diseases[10,11] and accumulate in the aged brain[5–9]. As such, we were determined to further investigate which specific T-cell subsets were altered in brain aging and if age-associated systemic factors were involved. Our data emphasizes above all the accumulation of effector and memory T cells with an exhausted phenotype in the aged circulation and brain, and shows that systemic exposure to aged plasma can induce migration and/or expansion of $CD8^+$ T cells in the brain parenchyma of young-adult mice. This connection between age-associated blood-born factors and $CD8^+$ T cell recruitment opens potential ways through which a possible $CD8^+$ T cell mediated decline in brain function can be counteracted via systemic modulation. Future research will have to determine routes of aged-plasma induced $CD8^+$ T cell migration and expansion within the brain, investigate their interaction with other brain resident cells and study long-term effects of exposure to age-associated systemic factors.

Methods

Animal model

Experiments were performed using male C57BL/6 wild-type (WT) mice (The Jackson Laboratory [strain C57BL/6J; stock number 000664; http://jaxmice.jax.org/). All animals were bred on location, handled regularly and group housed (max. 5) under standard laboratory conditions (12-hour light/dark cycle, 21°C, 50% humidity) in the presence of cage enrichment (nesting material). Water and food were available ad libitum. Experiments were reviewed and approved by the Animal Ethics Committee of the Central

Authority for Scientific Experiments on Animals of the Netherlands (CCD, approval protocol AVD115002016659), and acting in accordance with the Directive of the European Parliament and of the Council of the European Union of September 22nd 2010 (2010/63/EU).

Plasma collection and injection

Mouse plasma was collected from WT mice (average age 20 months +/- 2 months). Mice were euthanized using Euthanimal, then plasma was collected by intracardial bleed at time of sacrifice. Plasma was prepared from blood collected with edetic acid followed by centrifugation at 1000g for 10 min at 4°C (brake 1). Plasma aliquots were stored at −80°C until further use. Prior to administration, plasma was pooled and dialyzed using 3.5-kDa Slide-A-Lyzer Dialysis Cassettes (Thermo Scientific) in PBS to remove edetic acid (2x 2 hour at RT, and 1x o/n at 4°C in 4 L PBS). WT mice were systemically treated with 8 plasma injections (150 µL), or with PBS injections as control, intravenously via the tail vein over a period of 28 days, starting at 5 months of age (± 1 week). Mice were sacrificed the day after the last plasma injection for immune cell isolations. Mice used in immunohistochemical analyses received after the last day of plasma treatment, intraperitoneal injections of BrdU (150mg/kg in PBS; Thermo Fisher) for 3 consecutive days and were directly sacrificed the day after the last BrdU injection.

Immune cell isolations from brain, spleen and blood

Tissue collection

Mice were first euthanized using Euthanimal. Blood was collected by intracardial bleed at time of sacrifice with a needle containing edetic acid via the right ventricle. Trans-cardinal perfusion was performed through the left ventricle with a peristaltic pump using PBS (no $Ca2^+$ or $Mg2^+$) for 5 min (3 mL/min). After perfusion, mice were decapitated and the brain and spleen were removed. For the 6-month-old “young-adult” and 20 month-old “aged” mice, total brain was used for immune cell isolation and subsequent CyTOF analysis. For the plasma or PBS-treated animals, cortical and hippocampal brain structures were removed prior isolation. Finally, tissues were stored in in RPMI (RPMI 1640, Thermo Fisher) on ice until further processing.

Spleen and brain dissection and digestion

Spleens and brains were transferred to a 24-well plate and thoroughly dissected with sharp scissors in 1 mL of digestive mix (2 U/mL Liberase TL, #5401020001). The 1 mL cell suspension was transferred to 12-mL round bottom polypropylene tubes containing 1 mL of 2 U/mL Liberase TL. A magnetic stirrer was added to each tube and the suspensions were incubated in a 37ºC stove on a magnetic stir plate at 200 RPM for 20 min (spleen) and 50 min (brain). Then, 10 mL of ice-cold RPHE (RPMI 1640, 10% FCS, 10 mM EDTA, 20 mM HEPES, 50 µm 2-mercaptoethanol) was added to each tube and the tubes were put in a glass bucket containing ice on top of a stir plate and stirred for 10 min at 500 RPM. Next, the cell suspension was filtered through a 70 µm cell strainer into a 50-mL canonical tube and 30 mL of RP10 (RPMI 1640, 10% FCS, 1% penicillin/streptomycin, 1% glutamine) was added.

Spleen processing

Splenocytes were then centrifuged for 7 min at 1500 RPM, brake 5. The pellet was resuspended in 5 mL ACK red blood cell lysis buffer (Thermo Fisher), transferred to a 15 mL tube and incubated for 5 min on room temperature (RT) with occasional shaking. Next, 8 mL of RP10 was added and samples were centrifuged for 7 min at 1500 RPM, brake 5. Supernatant was carefully removed. Cell pellets were suspended in 1 mL RP10 for counting followed by cell viability staining.

Brain processing

Myelin was separated and removed from the brain using a density gradient. The pellet was resuspended in 70% Percoll, and 30% Percoll was carefully layered on top. Following centrifugation at 900g for 30 min at 22ºC, immune cells in the 70-30% interphase were collected into 10 mL of RP10 buffer. Cell pellets were suspended in 1 mL RP10 for counting followed by cell viability staining.

Blood processing

Blood samples were centrifuged at 300g for 10 min (9 acc/6 dec) at 4ºC. Plasma was removed from the upper layer and remaining blood samples were transferred to a 15 mL tube and 5 mL ACK red blood cell lysis buffer (Thermo Fisher) was added. Samples were incubated for 5 min on RT with occasional shaking. Next, 8 mL of RP10 was added and samples were centrifuged for 7 min at 1500 RPM, brake 5. Supernatant was carefully removed and samples underwent another round of red blood cell lysis. Then, 10 mL of RP10 was added to the samples and centrifuged 7 min at 1500 RPM, brake 5. Cell pellets were suspended in 1 mL RP10 for counting followed by cell viability staining.

CyTOF viability staining, fixation and freezing of immune cells

Isolated immune cells were washed with HBSS-/- (without Mg^{+2}, Ca^{+2} and phenol red). Cells were distributed in wells of a 96-well V-bottom plate, washed with Maxpar PBS (Fluidigm, #201058) and stained with the viability marker Cell-ID™ Cisplatin-198Pt (Fluidigm, #201198) for 5 min at 37°C according to the manufacturer's instructions. Cells were then washed with RP10 and fixed with Maxpar Fix I Buffer (Fluidigm, #201065) for 10 min at RT. Fixed cells were centrifuged at 800g for 7 min at 4°C. Cell pellets were resuspended in 10% DMSO/FCS and put in a Mr Frosty Freezing Container at -80°C for 24 h. Samples were stored at -80°C until staining and sample acquisition.

CyTOF antibody labeling and titration

Antibody labelling with the indicated metal tag was performed using the MaxPAR antibody conjugation kit (Fluidigm) according to the manufacturer's instructions. Purification of the bound antibody was performed with high-performance liquid chromatography (Thermo Fisher) and subsequently concentrated by filtering with a 10-kDa filter (Merck Millipore) in a swing-out bucket at 4000 RPM for 15 min. The end volume was determined and an equal volume of antibody stabilizer buffer (Fluidigm; supplemented with 0.05% sodium azide) was added before the antibodies were stored at 4°C. All antibodies used in this

study were titrated using both fixed and unfixed thawed immune cells and the most optimal concentrations with the least spillover were chosen.

CyTOF staining

Reagents were cooled on ice, centrifugation steps were performed at 800g for 7 min at 4°C (9 acc/7 dec) and incubations were performed at RT. Samples were thawed rapidly and washed twice with 8 mL of Maxpar PBS (Fluidigm) and transferred to a 96 well V-bottom plate. After centrifugation, cells were washed twice with 150 µL of 1X Barcode Perm Buffer (Fluidigm, #201057) and incubated with the appropriate palladium barcodes (Fluidigm, #201060) in 1X Barcode Perm Buffer for 30 min. After centrifugation, samples were washed twice with 150 µL of cell staining buffer (CSB) (Fluidigm, #201068) and the cells from all samples were pooled. Cells in this combined sample were counted and after centrifugation incubated with TruStain FcX anti-mouse CD16/32 (BioLegend, #101320) diluted in CSB (1:100) for 10 min. Surface antibody cocktails (Table 1) were prepared fresh in CSB and added to the combined sample in a cell to antibody-cocktail ratio of 3 x 10^6 cells per 100 uL. This was followed by a 30 min incubation. After the incubation cells were washed twice with CSB, followed by a wash with Maxpar PBS. Then, cells were fixated with 1 mL of freshly made 1.6% PFA (Thermo Fisher, #28906) in Maxpar PBS for 10 min. After centrifugation, cells were permeabilized with 1 mL of FoxP3 Fix/Perm working solution (eBioscience, #00-5523) for 30 min, followed by two washes with 1X Permeabilisation Buffer (eBioscience, #00-5523). Then, a freshly prepared nuclear antibody cocktail (Table 1) in 1X Permeabilisation Buffer was added in a cell to antibody-cocktail ratio of 3 x 10^6 cells per 100 uL and incubated for 45 min. Cells were then washed three times with 1X Permeabilisation Buffer and fixated with 1 mL of freshly made 1.6% PFA in Maxpar PBS for 10 min. After centrifugation, nucleated cells were stained with Maxpar Intercalator (Fluidigm, #201192B) diluted 1:4000 in Maxpar Fix and Perm Buffer (Fluidigm, #201067) and incubated overnight at 4°C, until sample acquisition.

Table 1: Antibodies for CyTOF

Metal	Target	Clone	Concentration (uL) *per* 100 uL	Cell marker *or* function	Cocktail
141Pr	Ly-6G/C (Gr-1)	RB6-8C5	0.05	neutrophils	surface
142Nd	KLRG1	2F1/KLRG1	1	exhausted T cells	surface
143Nd	CD11a/CD18	H155-78	0.5	integrin	surface
144Nd	MHC II	M5/114.15.2	0.03	APCs	surface
145Nd	CD4	RM45	0.5	$CD4^+$ T cells	surface
146Nd	CD138	281-2	0.5	plasma cells	surface
147Sm	CD36	72-1	1	fatty acid metabolism	surface
148Nd	CD11b	M1/70	0.05	myeloid cells	surface
149Sm	CD19	6D5	0.5	B cells	surface
150Nd	Ly-6C	HK1.4	0.1	monocytes, pDCs, $CD8^+$ T cells	surface
151Eu	CD64	X54-5/7.1	1	monocytes, macrophages	surface
152Sm	CD3e	145-2C11	0.5	T cells, NKT cells	surface
153Eu	CD38	90	0.05	B cells & activated T cells	surface
154Sm	TER-119 (Glycophorin A)	TER-119	0.5	*Red blood cells*	surface
155Gd	CD274 (PD-L1)	10F.9G2	0.1	immune checkpoint	surface
156Gd	F4/80	BM8	1	macrophages, eosinophils	surface
158Gd	FoxP3	FJK-16s	2	regulatory T cells	nuclear
159Tb	CD279 (PD-1)	J43	0.1	immune checkpoint	surface
160Gd	CD5	53-7.3	0.05	B & T cells	surface
161Dy	Tbet	4B10	1.5	T cells (marks Th1), NKT cells, B cells (subset)	nuclear
162Dy	TCRgd	GL3	0.2	T cells with TCR γ/δ	surface
163Dy	BCL6	K112-91	2	Tfh cells, GC B cells	nuclear
164Dy	CX3CR1	SA011F11	0.1	monocytes, macrophages, T cells	surface
165Ho	NK1.1	PK136	0.5	NK cells, NKT cells	surface
166Er	TIGIT	1G9	7	immune checkpoint	surface
167Er	Gata3	TWAJ	2	T cells (marks Th2)	nuclear

168Er	CD8a	53-6.7	0.5	CD8 T cells	surface
169Tm	TCRb	H57-597	0.5	T cells with TCR α/β	surface
170Er	CD45R (B220)	RA3-6B2	0.1	B cells	surface
171Yb	CD44	IM7	0.05	effector & memory T cells	surface
172Yb	Ki-67	B56	1	cell proliferation	nuclear
173Yb	CD103	2E7	1	T cells (marks Trm), DCs	surface
174Yb	CD223 (LAG3)	C9B7W	1	immune checkpoint	surface
175Lu	CD127 (IL-7Ra)	A7R34	2	naive & memory T cells	surface
176Yb	CD278 (ICOS)	7E17G9	1	immune checkpoint	surface
209Bi	CD11c	N418	0.05	DCs and monocytes	surface
89Y	CD45	30-F11	1	immune cells	surface

CyTOF sample acquisition

Cells in Maxpar Intercalator solution were washed twice with CSB and divided over approximately 1 x 10^6 cells per tube, followed by washing with Milli-Q water right before acquisition. Samples were filtered and calibration beads (Fluidigm, #201078) were added to the suspension to 15% of the final volume. Cells were acquired on a Helios™ (Fluidigm), with an event rate of 250 – 350 events per second in Milli-Q water. Runs took approximately 30 – 45 min. During the day, tuning of the machine was performed during start-up and after 4 hours of sample acquisition. Within each barcoded set of samples, one reference sample was included to correct for differences in staining intensity between barcodes due to technical variation in the staining protocol or daily changes in instrument functioning, as will be discussed later.

Generation of the CyTOF reference sample

The reference sample contained a mixture of immune cells derived from the mouse spleen, blood, brain, liver, bone-marrow and tumor biopsies. Part of the spleen and bone-marrow-derived immune cells were stimulated with 30 ng/mL PMA and 1 µg/mL ionomycin (both Sigma-Aldrich) for 120 min at 37°C to induce expression of transcription factors that were included in the CyTOF panel. All cells were combined, stained for viability as described earlier, fixated and stored in aliquots at -80°C until further use.

CyTOF data analysis

Acquired samples were randomized using Gaussian negative half zero randomization in CyTOF Software version 6.7. The FCS files were normalized using bead normalization, concatenated and debarcoded using the CyTOF Software version 6.7. Batch alignment for blood and spleen samples was then performed using CytoNorm[49] for each tissue and experiment (e.g. young/old and PBS/plasma-injected)

separately. This batch alignment however induced noise in the staining of the brain samples and so the decision was made to work with the ‘raw’ data there instead. The processed FCS files were then uploaded into OMIQ data analysis software (http://www.omiq.ai) and data analysis was performed. First, normalization beads, cell debris and cell doublets were removed from the data using the DNA staining, bead intensity and Gaussian parameters. Next, live cells showing negative reactivity for viability marker Cell-ID™ Cisplatin-198Pt and dim-to-positive reactivity for CD45-89Y were selected and used for further processing steps. Data were visualized in UMAPs and tSNEs and cells were appointed to clusters by Phenotyping by Accelerated Refined Community[21] (PARC) and PhenoGraph[50] algorithms. Visual inspection of 1) PARC- and PhenoGraph-derived clusters overlaid on corresponding UMAPs and tSNEs derived from the same sample, and 2) clustered heatmaps that compare median marker expression between clusters, guided the manual merging of clusters and their annotation into biologically relevant immune cell subsets. After the ‘general’ immune analysis, T cell clusters (and for some instances myeloid clusters as well) were selected, merged and subsampled after which the cluster analysis was repeated to ensure optimal resolution of the underlying data. Counts per immune cell subset were then exported and further analyzed in Graphpad Prism 8.2.1.

Immunofluorescence

After perfusion, mice were decapitated and brains were isolated for post-fixation overnight in 4% PFA (4°C) and subsequent incubation for 48 hours in 30% sucrose in PBS solution (4°C) and stored at -80°C. In addition, per mouse, 20 µm thick coronal sections were collected and mounted on Superfrost glass slides (Menzel-glaser, Germany) stored at -20C. For the staining, antigen retrieval was performed at 95°C for 30 min in sodium citrate (pH 6). Sections were incubated with either neutralized donkey serum, neutralized goat serum or neutralized rabbit serum for 30 min at RT. Sections were incubated overnight with primary antibodies in PBS (Table 2) at 4^{o}C. After incubation, the sections were stained with the appropriate secondary antibodies in PBS. Last, sections were counterstained with DAPI 1:10000 (DAKO) for 10 min.

Table 2: Antibodies for immunofluorescence

Antigen	Species	Dilution	Manufacturer	Cat. Number
CD45	Rat	1:200	BD Pharmingen	553076
CD4	Rabbit	1:250	Abcam	Ab217344
CD8	Rabbit	1:250	Abcam	Ab183685
Collagen IV / Coll-IV	Rabbit	1:200	Abcam	Ab6581
VCAM-1 / CD106	Rat	1:100	In house generated	
ICAM-1 / CD54	Rat	1:100	Biolegend	116101
PECAM-1 / CD31	Mouse	1:200	Abcam	Ab24590
Fibrinogen	Rabbit	1:200	DAKO	F0111
BrdU	Mouse	1:100	Invitrogen	14-5071-82
IBA1	Goat	1:500	Abcam	ab5076
P2Y12	Rabbit	1:500	AnaSpec	55043A
Lamp1	Rat	1:100	Biolegend	
HuC/D	Mouse	1:100	ThermoFisher Scientific	A21271
Homer1	Rabbit	1:500	Synaptic Systems	160 002

Microscopy and data analysis

T cell infiltration in the brain

Per mouse, minimal one complete coronal brain section was imaged using a wide-field microscope (Nikon TI2) at a 1.39 µm/pixel resolution. The $CD45^+$ $CD4^+$ and $CD45^+$ $CD8^+$ T cells were manually counted by a blinded observer and normalized to the total slide area. T cells inside the vessel and the meninges, visualized with Coll-IV, were excluded from the analysis.

Expression of cell adhesion molecules on the brain vasculature

Per mouse, 4 confocal images were obtained on a Leica TCS SP8 HyD confocal microscope using a 0.63 µm/pixel resolution, a z-stepsize of 0.33 µm and a total of 10 z-steps. The 3 µm depth z-stack was compressed into one 2D-image using a maximum projection. The percentage of positive vessels was determined using NIS Elements (Nikon) by dividing the total number of Coll-IV^+ and ICAM-1^+ / VCAM-1^+ / PECAM-1^+ vessels by the total number of Coll-IV^+ vessels. Thresholds were manually set per ROI by a blinded observer. Vessel density was determined by measuring and dividing the total Coll-IV^+ area by the total measured tissue area.

Blood vessel permeability

Per mouse, 4 confocal images were obtained on a Leica TCS SP8 HyD confocal microscope using a 0.18 µm/pixel resolution, a z-stepsize of 0.33 µm and a total of 10 z-steps. The 3 µm depth z-stack was compressed into one 2D-image using a maximum projection. Brain vessel permeability was determined by studying the area of extravascular fibrinogen. First, using NIS Elements (Nikon), a threshold was set manually per ROI by a blinded observer for both Coll-IV and fibrinogen. Per image, only the fibrinogen^{+} Coll-IV^{-} area outside the vessels was measured and normalized to the total amount of Coll-IV^{+} vessel area.

Microglial phenotype, number and proliferation

Per mouse, two widefield images were acquired on a Vectra 3.0 spectral imaging system (PerkinElmer) using a resolution of 0.497 µm/pixel. Sections labeled for IBA1 together with P2Y12 and BrdU were analyzed using NIS Elements (Nikon). In short, mean fluorescence intensity of P2Y12 in microglia was quantified by measuring the total fluorescence intensity of P2Y12 within the IBA1^{+} mask. Microglia density and proliferation was determined by manually counting the number of IBA1^{+} and IBA1^{+} BrdU^{+} cells per area by a blinded observer.

Microglial morphology

Per mouse, 10 confocal images were obtained on a Leica TCS SP8 HyD confocal microscope using a 0.09 µm/pixel resolution, a z-stepsize of 0.3 µm and a total of 11 z-steps. The 3 µm depth z-stack was compressed into one 2D-image using a maximum projection. Each z-stack contained one IBA1^{+} cell located in the stratum radiatum of the hippocampus. IBA1^{+} microglia were manually traced using FIJI (NIH). Traced microglia were analyzed using the Sholl Analysis Plugin[51] with a 0.2 µm step size from the cell soma. Soma surface area of the traced microglia was measured using the freehand selection tool in FIJI.

Neuronal cell count

Per mouse, two widefield images of HuC/D stained sections were acquired on a Vectra 3.0 spectral imaging system (PerkinElmer) using a resolution of 0.497 µm/pixel. Cortical neuronal density was determined by manually counting the number of HuC/D^{+} cells per cortical area by a blinded observer.

Synapse density and pruning

Per mouse, 10 confocal images each containing one IBA1^{+} cell using a 0.09 µm/pixel resolution, a z-stepsize of 0.3 µm and a total of 11 z-steps, were acquired from the stratum radiatum area of the hippocampus. To measure synaptic density, Homer1^{+} spots were created using NIS Elements (Nikon) with a spot diameter of 0.5 µm in a manually selected area lacking IBA1^{+} cellular processes or cell nuclei. The density of Homer1^{+} spots was then calculated by dividing the number of spots by the total volume of

the selected region. To investigate synaptic pruning by microglia, manual thresholds were set for Lamp1 and IBA1 to obtain only Lamp1$^+$ IBA1$^+$ volumes. Next Homer1$^+$ spots located within the Lamp1$^+$ IBA1$^+$ volumes were counted. Lysosomal size was calculated by dividing the total Lamp1$^+$ IBA1$^+$ volume by the total IBA1$^+$ volume.

Statistics

Graphpad Prism 8.2.1 was used for all statistical tests. Shapiro–Wilk and F tests were performed to test for normality and equality of variances, respectively, after which appropriate tests were selected. The unpaired two-tailed Student's t test with or without Welch's correction for unequal variances for normally distributed data, or the Mann–Whitney test for non-normally distributed data. To examine the strength of association between two variables, either Pearson or Spearman correlation was used depending on the normality of the data. Data were judged to be statistically significant when $P < 0.05$ and, if significant, reported in the figures using the significance levels indicated in the figure legends.

References

1. Guerrero, A., De Strooper, B. & Arancibia-Carcamo, I. L. Cellular senescence at the crossroads of inflammation and Alzheimer's disease. *Trends Neurosci* **44**, 714–727, doi:10.1016/j.tins.2021.06.007 (2021).
2. Franceschi, C. *et al.* Inflamm-aging. An evolutionary perspective on immunosenescence. *Ann N Y Acad Sci* **908**, 244–254, doi:10.1111/j.1749-6632.2000.tb06651.x (2000).
3. Korin, B. *et al.* High-dimensional, single-cell characterization of the brain's immune compartment. *Nat Neurosci* **20**, 1300–1309, doi:10.1038/nn.4610 (2017).
4. Mrdjen, D. *et al.* High-Dimensional Single-Cell Mapping of Central Nervous System Immune Cells Reveals Distinct Myeloid Subsets in Health, Aging, and Disease. *Immunity* **48**, 380-395 e386, doi:10.1016/j.immuni.2018.01.011 (2018).
5. Smolders, J. *et al.* Tissue-resident memory T cells populate the human brain. *Nat Commun* **9**, 4593, doi:10.1038/s41467-018-07053-9 (2018).
6. Ritzel, R. M. *et al.* Age-Associated Resident Memory CD8 T Cells in the Central Nervous System Are Primed To Potentiate Inflammation after Ischemic Brain Injury. *J Immunol* **196**, 3318–3330, doi:10.4049/jimmunol.1502021 (2016).
7. Moreno-Valladares, M. *et al.* CD8(+) T cells are increased in the subventricular zone with physiological and pathological aging. *Aging Cell* **19**, e13198, doi:10.1111/acel.13198 (2020).
8. Moreno-Valladares, M. *et al.* CD8(+) T cells are present at low levels in the white matter with physiological and pathological aging. *Aging (Albany NY)* **12**, 18928–18941, doi:10.18632/aging.104043 (2020).
9. Dulken, B. W. *et al.* Single-cell analysis reveals T cell infiltration in old neurogenic niches. *Nature* **571**, 205–210, doi:10.1038/s41586-019-1362-5 (2019).

10. Unger, M. S. *et al.* CD8(+) T-cells infiltrate Alzheimer's disease brains and regulate neuronal- and synapse-related gene expression in APP-PS1 transgenic mice. *Brain Behav Immun* **89**, 67–86, doi:10.1016/j.bbi.2020.05.070 (2020).
11. Gate, D. *et al.* Clonally expanded CD8 T cells patrol the cerebrospinal fluid in Alzheimer's disease. *Nature* **577**, 399–404, doi:10.1038/s41586-019-1895-7 (2020).
12. Hao, Y., O'Neill, P., Naradikian, M. S., Scholz, J. L. & Cancro, M. P. A B-cell subset uniquely responsive to innate stimuli accumulates in aged mice. *Blood* **118**, 1294–1304, doi:10.1182/blood-2011-01-330530 (2011).
13. Kim, K. *et al.* Therapeutic B-cell depletion reverses progression of Alzheimer's disease. *Nat Commun* **12**, 2185, doi:10.1038/s41467-021-22479-4 (2021).
14. Lehallier, B. *et al.* Undulating changes in human plasma proteome profiles across the lifespan. *Nat Med* **25**, 1843–1850, doi:10.1038/s41591-019-0673-2 (2019).
15. Villeda, S. A. *et al.* The ageing systemic milieu negatively regulates neurogenesis and cognitive function. *Nature* **477**, 90–94, doi:10.1038/nature10357 (2011).
16. Yousef, H. *et al.* Aged blood impairs hippocampal neural precursor activity and activates microglia via brain endothelial cell VCAM1. *Nat Med* **25**, 988–1000, doi:10.1038/s41591-019-0440-4 (2019).
17. De Miguel, Z. *et al.* Exercise plasma boosts memory and dampens brain inflammation via clusterin. *Nature* **600**, 494–499, doi:10.1038/s41586-021-04183-x (2021).
18. Castellano, J. M. *et al.* Human umbilical cord plasma proteins revitalize hippocampal function in aged mice. *Nature* **544**, 488–492, doi:10.1038/nature22067 (2017).
19. Villeda, S. A. *et al.* Young blood reverses age-related impairments in cognitive function and synaptic plasticity in mice. *Nat Med* **20**, 659–663, doi:10.1038/nm.3569 (2014).
20. Middeldorp, J. *et al.* Preclinical Assessment of Young Blood Plasma for Alzheimer Disease. *JAMA Neurol* **73**, 1325–1333, doi:10.1001/jamaneurol.2016.3185 (2016).
21. Stassen, S. V. *et al.* PARC: ultrafast and accurate clustering of phenotypic data of millions of single cells. *Bioinformatics* **36**, 2778–2786, doi:10.1093/bioinformatics/btaa042 (2020).
22. Hartmann, F. J. *et al.* Single-cell metabolic profiling of human cytotoxic T cells. *Nat Biotechnol* **39**, 186–197, doi:10.1038/s41587-020-0651-8 (2021).
23. Katsuyama, E. *et al.* The CD38/NAD/SIRTUIN1/EZH2 Axis Mitigates Cytotoxic CD8 T Cell Function and Identifies Patients with SLE Prone to Infections. *Cell Rep* **30**, 112-123 e114, doi:10.1016/j.celrep.2019.12.014 (2020).
24. Philip, M. *et al.* Chromatin states define tumour-specific T cell dysfunction and reprogramming. *Nature* **545**, 452–456, doi:10.1038/nature22367 (2017).
25. Li, D. Y. & Xiong, X. Z. ICOS(+) Tregs: A Functional Subset of Tregs in Immune Diseases. *Front Immunol* **11**, 2104, doi:10.3389/fimmu.2020.02104 (2020).
26. Lowther, D. E. *et al.* PD-1 marks dysfunctional regulatory T cells in malignant gliomas. *JCI Insight* **1**, doi:10.1172/jci.insight.85935 (2016).

27. Wu, Z. CX3CR1(+) B cells show immune suppressor properties. *J Biol Chem* **289**, 22630–22635, doi:10.1074/jbc.M114.569459 (2014).
28. Lund, F. E., Yu, N., Kim, K. M., Reth, M. & Howard, M. C. Signaling through CD38 augments B cell antigen receptor (BCR) responses and is dependent on BCR expression. *J Immunol* **157**, 1455–1467 (1996).
29. Gary-Gouy, H. *et al.* Human CD5 promotes B-cell survival through stimulation of autocrine IL-10 production. *Blood* **100**, 4537–4543, doi:10.1182/blood-2002-05-1525 (2002).
30. Carrasco, Y. R., Fleire, S. J., Cameron, T., Dustin, M. L. & Batista, F. D. LFA-1/ICAM-1 interaction lowers the threshold of B cell activation by facilitating B cell adhesion and synapse formation. *Immunity* **20**, 589–599, doi:10.1016/s1074-7613(04)00105-0 (2004).
31. Shekhar, K., Brodin, P., Davis, M. M. & Chakraborty, A. K. Automatic Classification of Cellular Expression by Nonlinear Stochastic Embedding (ACCENSE). *Proc Natl Acad Sci U S A* **111**, 202–207, doi:10.1073/pnas.1321405111 (2014).
32. Sallusto, F., Geginat, J. & Lanzavecchia, A. Central memory and effector memory T cell subsets: function, generation, and maintenance. *Annu Rev Immunol* **22**, 745–763, doi:10.1146/annurev.immunol.22.012703.104702 (2004).
33. Morris, A. B., Adams, L. E. & Ford, M. L. Influence of T Cell Coinhibitory Molecules on CD8(+) Recall Responses. *Front Immunol* **9**, 1810, doi:10.3389/fimmu.2018.01810 (2018).
34. Song, Y. *et al.* T-cell Immunoglobulin and ITIM Domain Contributes to CD8(+) T-cell Immunosenescence. *Aging Cell* **17**, doi:10.1111/acel.12716 (2018).
35. Bianchini, M. *et al.* PD-L1 expression on nonclassical monocytes reveals their origin and immunoregulatory function. *Sci Immunol* **4**, doi:10.1126/sciimmunol.aar3054 (2019).
36. Ginhoux, F. & Jung, S. Monocytes and macrophages: developmental pathways and tissue homeostasis. *Nat Rev Immunol* **14**, 392–404, doi:10.1038/nri3671 (2014).
37. Geissmann, F., Jung, S. & Littman, D. R. Blood monocytes consist of two principal subsets with distinct migratory properties. *Immunity* **19**, 71–82, doi:10.1016/s1074-7613(03)00174-2 (2003).
38. Baruch, K. *et al.* PD-1 immune checkpoint blockade reduces pathology and improves memory in mouse models of Alzheimer's disease. *Nat Med* **22**, 135–137, doi:10.1038/nm.4022 (2016).
39. Deczkowska, A. *et al.* Mef2C restrains microglial inflammatory response and is lost in brain ageing in an IFN-I-dependent manner. *Nat Commun* **8**, 717, doi:10.1038/s41467-017-00769-0 (2017).
40. Mohebiany, A. N. *et al.* Microglial A20 Protects the Brain from CD8 T-Cell-Mediated Immunopathology. *Cell Rep* **30**, 1585-1597 e1586, doi:10.1016/j.celrep.2019.12.097 (2020).
41. Daglas, M. *et al.* Activated CD8(+) T Cells Cause Long-Term Neurological Impairment after Traumatic Brain Injury in Mice. *Cell Rep* **29**, 1178-1191 e1176, doi:10.1016/j.celrep.2019.09.046 (2019).
42. Coque, E. *et al.* Cytotoxic CD8(+) T lymphocytes expressing ALS-causing SOD1 mutant selectively trigger death of spinal motoneurons. *Proc Natl Acad Sci U S A* **116**, 2312–2317, doi:10.1073/pnas.1815961116 (2019).

43. Chevalier, G. *et al.* Neurons are MHC class I-dependent targets for CD8 T cells upon neurotropic viral infection. *PLoS Pathog* **7**, e1002393, doi:10.1371/journal.ppat.1002393 (2011).
44. Di Liberto, G. *et al.* Neurons under T Cell Attack Coordinate Phagocyte-Mediated Synaptic Stripping. *Cell* **175**, 458-471 e419, doi:10.1016/j.cell.2018.07.049 (2018).
45. Garber, C. *et al.* T cells promote microglia-mediated synaptic elimination and cognitive dysfunction during recovery from neuropathogenic flaviviruses. *Nat Neurosci* **22**, 1276–1288, doi:10.1038/s41593-019-0427-y (2019).
46. Krasemann, S. *et al.* The TREM2-APOE Pathway Drives the Transcriptional Phenotype of Dysfunctional Microglia in Neurodegenerative Diseases. *Immunity* **47**, 566-581 e569, doi:10.1016/j.immuni.2017.08.008 (2017).
47. Peng, J. *et al.* Microglial P2Y12 receptor regulates ventral hippocampal CA1 neuronal excitability and innate fear in mice. *Mol Brain* **12**, 71, doi:10.1186/s13041-019-0492-x (2019).
48. Rebo, J. *et al.* A single heterochronic blood exchange reveals rapid inhibition of multiple tissues by old blood. *Nat Commun* **7**, 13363, doi:10.1038/ncomms13363 (2016).
49. Van Gassen, S., Gaudilliere, B., Angst, M. S., Saeys, Y. & Aghaeepour, N. CytoNorm: A Normalization Algorithm for Cytometry Data. *Cytometry A* **97**, 268–278, doi:10.1002/cyto.a.23904 (2020).
50. Levine, J. H. *et al.* Data-Driven Phenotypic Dissection of AML Reveals Progenitor-like Cells that Correlate with Prognosis. *Cell* **162**, 184–197, doi:10.1016/j.cell.2015.05.047 (2015).
51. Ferreira, T. A. *et al.* Neuronal morphometry directly from bitmap images. *Nat Methods* **11**, 982–984, doi:10.1038/nmeth.3125 (2014).

Declarations

Acknowledgments

We thank dr. Juan J. Garcia Vallejo and Cora Chadick for managing the O2Flow cytometry facility within the MCCF Advanced Microscopy and Cytometry Research Core Facility at the Amsterdam UMC and Jan Verhoeff for technical assistance at the CyTOF Helios and data analysis. Also, thanks to the 'Single cEllga' group members Carla Rodriguez-Mogeda and Sabela Rodriguez Lorenzo for their support during the data analysis and review of the final manuscript. Special thanks to Sjoerd T.T. Schetters for his experimental advice, thoughtful discussions and the willingness to share related mouse research. We thank Christiaan Huffels for his assistance during the perfusions of the mice. This work was funded by ZonMw, The Netherlands Organisation for Health Research and Development, Dementia Research and Innovation Program "Memorabel" with additional support from Alzheimer Nederland (733050504 - JM), by UMC Utrecht Rudolf Magnus Young Talent fellowship 2017 (JM) and by Horizon 2020 (686009 - LO, MS and HV).

Author contributions

J.M. conceived and started the initial study with aged plasma injections and L.O. included the analysis of the immune system and build it into the final design as in the current manuscript. J.M., R.D. and D.V. maintained the mouse colony, collected and dialyzed aged plasma and performed the plasma injections. L.H. assisted with the mouse perfusions, and L.H. and R.D. cut the mouse brain tissue. L.O. and M.S. isolated immune cells from the mouse brain, blood and spleen. L.O. designed the CyTOF panel and S.P. conjugated the antibodies. L.O. and S.P. performed the sample staining for the CyTOF and running of the samples. L.O. independently analyzed the CyTOF data. A.K. performed microscopy analysis on the mouse brains, guided by L.O. and M.W. A.K. assisted L.O. with the layout of the figures. L.O. wrote the manuscript with guidance of M.W., J.M. and H.V. Funding and supervision of the study was provided by J.M. and H.V.

Figures

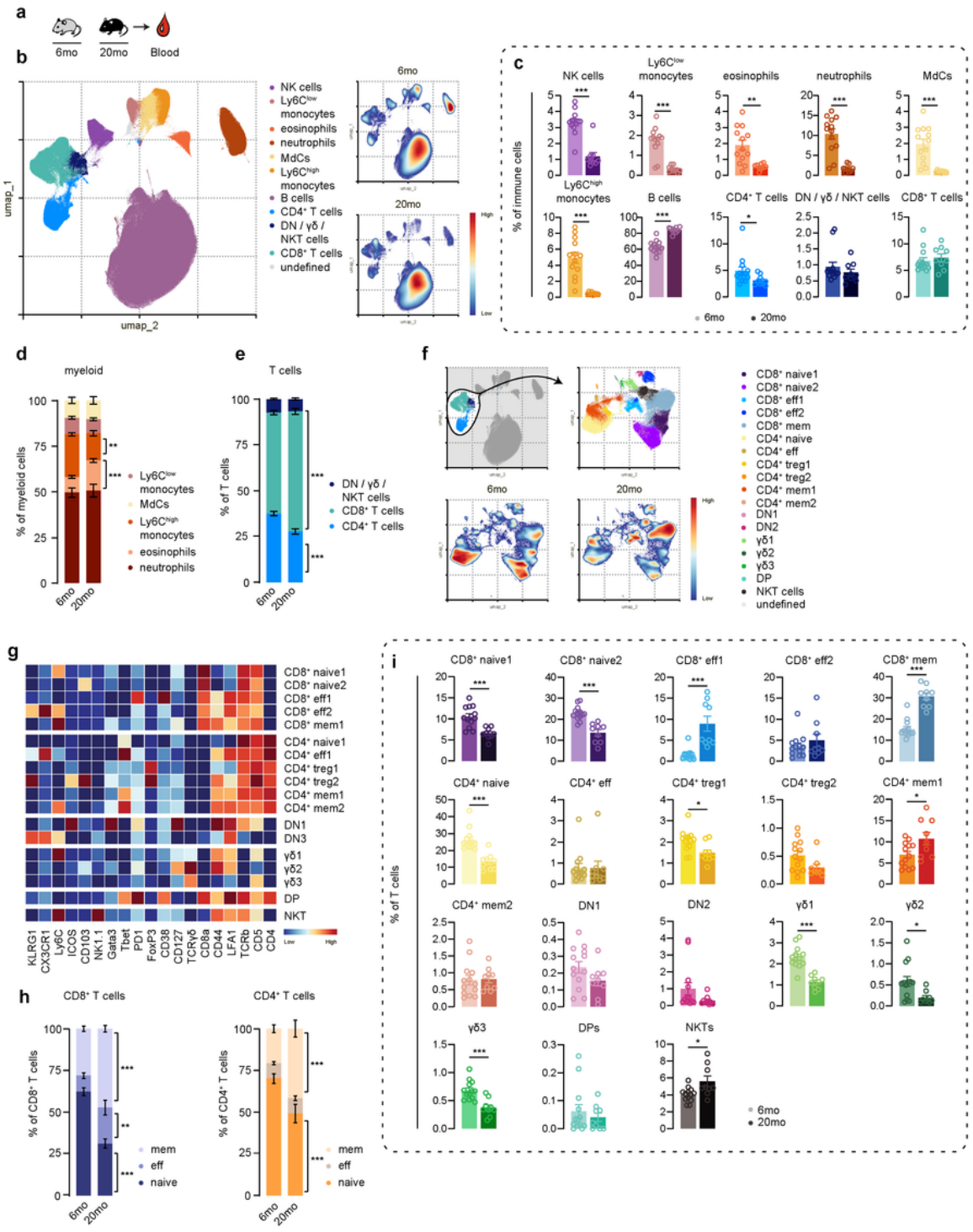

Figure 1

Figure legend not available with this version.

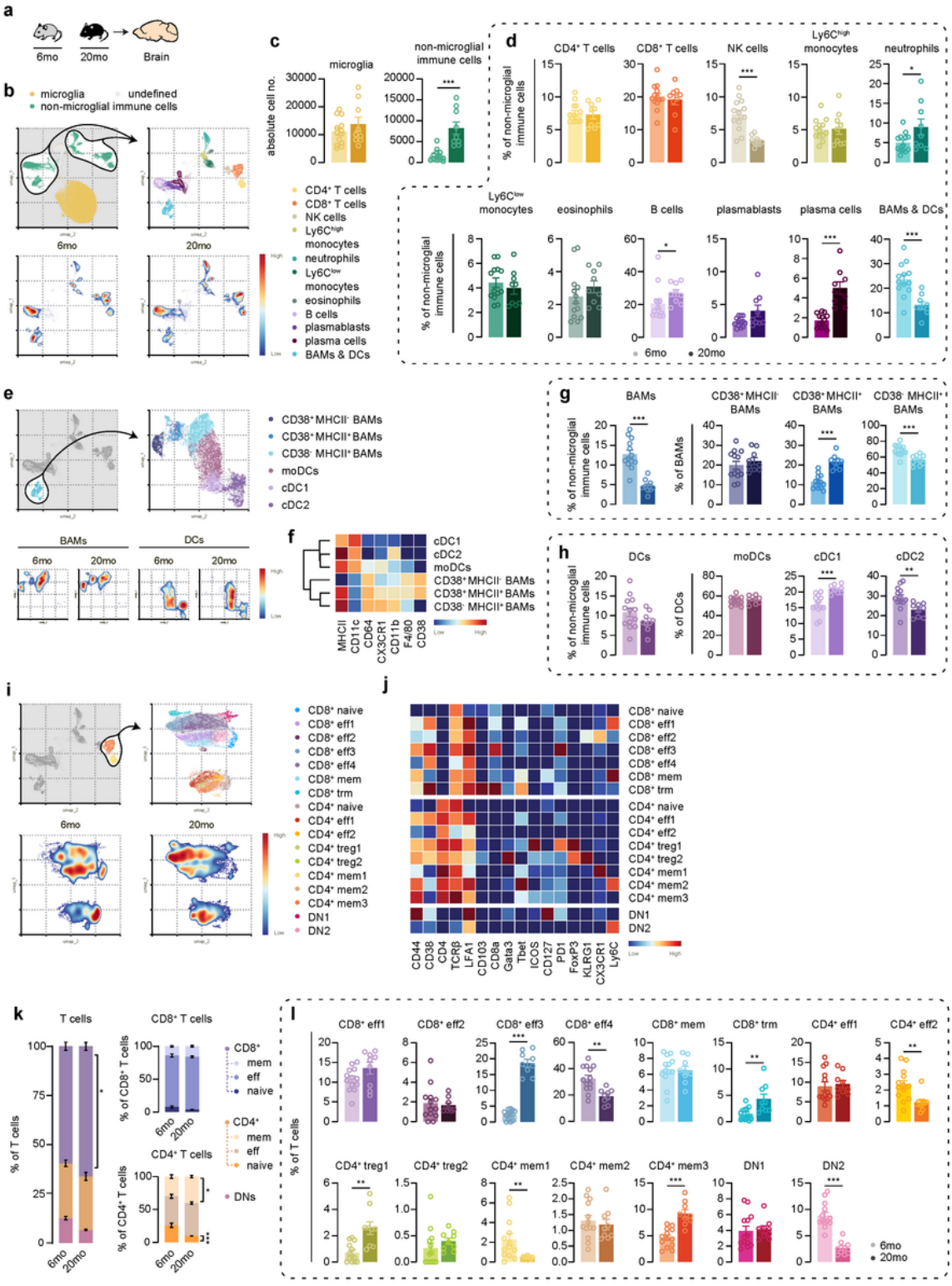

Figure 2

Figure legend not available with this version.

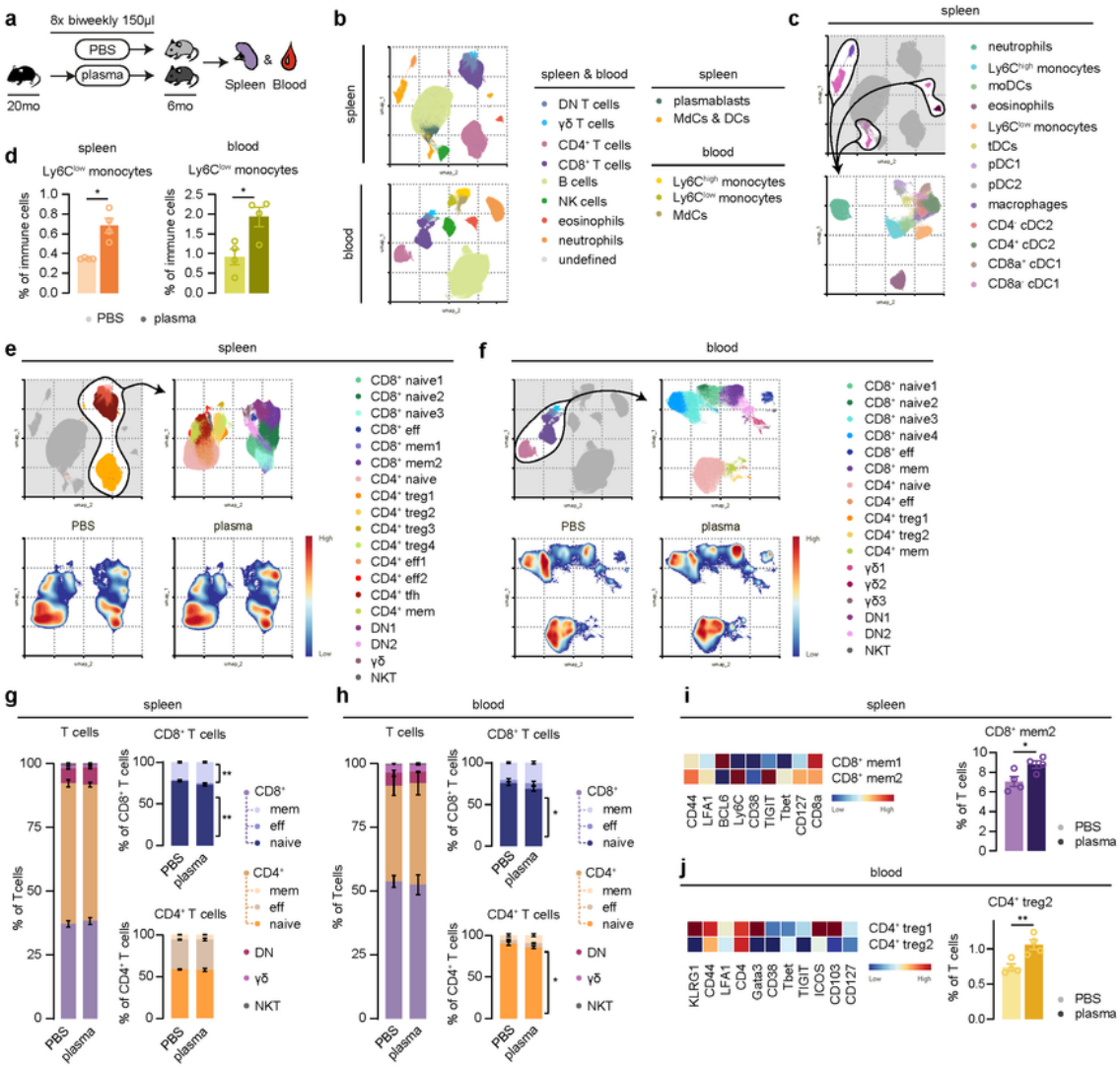

Figure 3

Figure legend not available with this version.

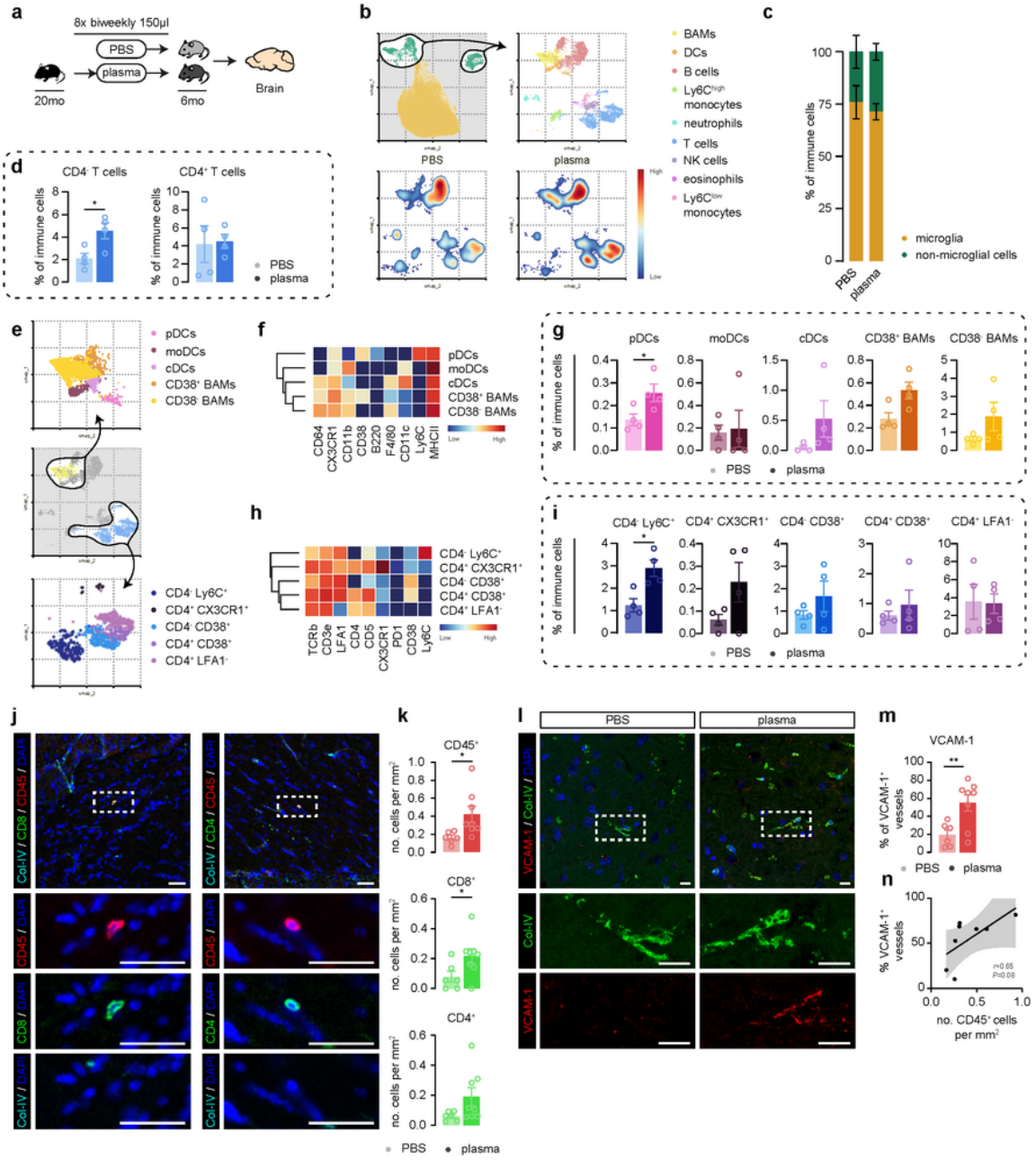

Figure 4

Figure legend not available with this version.

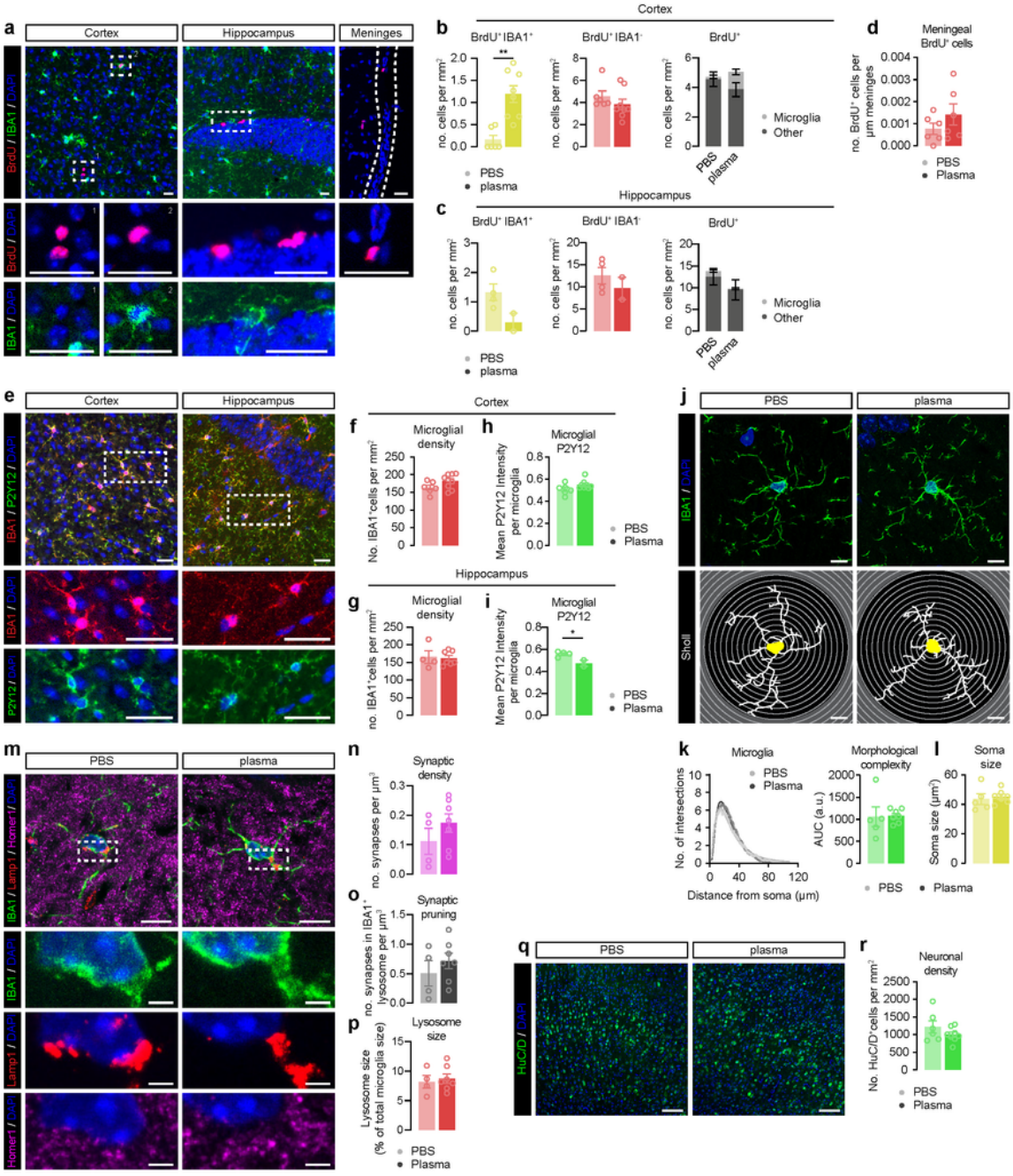

Figure 5

Figure legend not available with this version.

Supplementary Files

This is a list of supplementary files associated with this preprint. Click to download.

- FigS1.pdf
- FigS2.pdf
- FigS3.pdf
- FigS4.pdf